Processing and Application of Ceramics 14 [3] (2020) 181–187
https://doi.org/10.2298/PAC2003181N

ZrB_2 matrix composites with Cr^{3+}/Nd^{3+} doped Al_2O_3 luminescent nanoparticles for non-contact temperature sensing

Annamária Naughton-Duszová[1,*], Lukasz Marciniak[2,*], Aleksandra Dubiel[1,3], Jolanta Laszkiewicz-Łukasik[1], Karolina Kniec[2], Marcin Podsiadło[1]

[1]*Łukasiewicz Research Network – Krakow Institute of Technology, Zakopiańska 73, 30-418 Krakow, Poland*
[2]*Institute of Low Temperature and Structure Research, Polish Academy of Science, Okolna 2, Wroclaw 50-422, Poland*
[3]*AGH University of Science and Technology, Mickiewicza 30, Krakow 30-059, Poland*

Received 28 February 2020; Received in revised form 30 April 2020; Accepted 9 June 2020

Abstract

The effect of the addition of Cr^{3+}/Nd^{3+} doped Al_2O_3 nanoparticles (Al_2O_3 co-doped with 1% Cr^{3+} and 1% Nd^{3+} ions) on the mechanical and luminescent properties of ZrB_2 ceramic composites was investigated. ZrB_2 based composites with addition of 8, 16 and 32 wt.% of alumina nanoparticles were prepared by spark plasma sintering (SPS). Microstructure characteristics were studied by scanning electron microscopy (SEM), elastic modulus by ultrasonic wave transition method, hardness and fracture toughness by the Vickers indentation methods. The addition of alumina nanoparticles had positive effect on the mechanical properties of the composites. Thus, the hardness increased from 14.5 to 16.2 GPa and the fracture toughness from 3.91 to 5.89 MPa·$m^{1/2}$ in comparison to the values of the monolithic ZrB_2 system. The composite with the highest additive content showed evident luminescent character and the increase of the temperature caused a reduction of luminescent intensity. This is the first report which shows luminescent properties of ZrB_2 composites. Moreover, for the first time, luminescent properties of Cr^{3+} ions were used to develop ZrB_2 matrix composites with Cr^{3+}/Nd^{3+} doped Al_2O_3 particles with the self-temperature readout functionality via luminescent thermometry.

Keywords: *ceramic composites, ZrB_2, luminescent nanoparticles, microstructure development*

I. Introduction

There is a growing interest in ceramics and ceramic composites based on transition metals (Zr, Hf, etc.) mainly diborides, but also carbides, often referred to as ultra-high temperature ceramics (UHTCs). This is due to the unique combination of physical, thermal and mechanical properties, such as high refractoriness (melting points above 2500 °C), high electrical and thermal conductivity, chemical inertness against molten metals and slags and high resistance to ablation in oxidizing environments [1–4].

The unique properties of these materials enable their potential application in: military and thermonuclear reactor, parts of machines and devices, components of thermal protection, edges of attack in airplanes, as well as cutting tools [8]. The high melting point and oxidation resistance allow their use in the space industry, e.g. in jet engine nozzles [5–7]. The manufacturing processes and physico-mechanical properties of ceramics based on ZrB_2 have been extensively described in the literature [1,8,9]. With the aim to improve the densification, mechanical and physical properties, as well as the oxidation and ablation resistance of the ZrB_2 ceramics, the composite approach has been successfully adopted. The addition of SiC, $MoSi_2$ and $ZrSi_2$ significantly increased the room and high temperature strength, thermal and electrical conductivities of ZrB_2-based composites [8].

One important parameter which determines the lifetime of ceramic based elements and tools is the temperature distribution on their surface in real time. Fast and accurate determination of the temperature gradient and

*Corresponding author: tel: +55 79 3194 6344,
e-mail: *annamaria.duszova@kit.lukasiewicz.gov.pl* (Annámaria Naughton-Duszová), *l.marciniak@intibs.pl* (Lukasz Marciniak)

overheating spots may elongate their operating time if considered in the component design. Therefore, taking advantage of non-contact temperature sensing provided by the luminescent thermometry technique, it is possible to develop luminescent ceramic composites with self-temperature monitoring functionality. With the implementation of highly sensitive luminescent thermometers into ceramics it will be possible to analyse in real time the heat distribution on the ceramics. This kind of fast, accurate and easy spatial temperature analysis enables a far more efficient detection of overheating spots. This unique feature enables rapid and non-contact temperature readout of the elements made of such functional ceramics.

Recently luminescence nanothermometry has attracted great attention due to many possible applications [10,11]. One of the key parameters, which quantitatively defines the suitability of luminescent nanothermometers for real applications, is their relative sensitivity (S). The recently published reports presented different approaches to active modification of sensitivity, e.g. by changing the type and concentration of luminescent dopants, size of nanograins or by change of the excitation density or wavelength [12]. Al_2O_3 was selected as a host material due to the fact that it is well known for its high mechanical and thermal stability which is especially important in the case of the high annealing temperature used during sintering process. The Cr^{3+} ion is one of the best known and most extensively investigated transition metal ion whose optical properties are strongly affected by the temperature. Therefore emission intensity of Cr^{3+} ions may be used as a luminescent temperature probe. On the other hand, the Nd^{3+} luminescence, due to the characteristic configuration of energy levels of $4f$ orbitals, is expected to be less temperature dependent and may act as a luminescent reference. Therefore the luminescence intensity ratio of Cr^{3+} and Nd^{3+} ions is an efficient temperature dependent parameter which enables noncontact temperature readout.

There are some reports dealing with the transparent or translucent alumina doped with optically (photoluminescence) active rare earth and transition metal ions [12–14]. Bodišová *et al.* [13] prepared transparent/translucent rare earth (Eu, Er, Nd) doped alumina systems with photoluminescent properties by a combination of slip casting, pressureless pre-sintering and hot isostatic pressing (HIP). The luminescence properties of the RE-doped Al_2O_3 were comparable to other similar materials, e.g. doped alumina powders, making them a promising material for LED applications. Drdlíková *et al.* [14] processed transparent photoluminescent aluminas doped with 0.1–0.17 at.% Er with real in-line transmission values ranging between 28 and 56%. The samples doped with Er_2O_3 nano-powder exhibited slightly lower transparency due to the presence of Er agglomerates in the microstructure. Recently Eu/Ce doped MgO-Ga_2O_3-SiO_2 glasses and glass-ceramics- have been processed and characterized with different composition in different heat treatment atmospheres and temperatures [15].

The aim of the present contribution was to investigate the influence of the addition of Al_2O_3, doped with 1% Cr^{3+} and 1% Nd^{3+} on microstructure development, physical, mechanical and luminescent properties of ZrB_2 matrix ceramic composites.

II. Experimental method

This study used commercially available ZrB_2 powder (Grade B) with an average particle size of 1.5–3 μm. Zirconium diboride was provided by producer H.C. Starck. The ZrB_2 powder was prepared using Fritsch Pulverisette 6 planetary ball mill equipped with WC-Co grinding vessel and balls. The modified Pechini method has been successfully employed in the synthesis of Al_2O_3 nanomaterials doped with Cr^{3+} and Nd^{3+} ions. The Cr^{3+} and Nd^{3+} ions have been used in the concentration of 1% and 1% in respect to Al_3^+ ions. Neodymium oxide (Nd_2O_3 with 99.999% purity from Stan-ford Materials Corporation), chromium nitrate nonahydrate ($Cr(NO_3)_3 \cdot 9\,H_2O$ with 99.999% purity from Alfa Aesar), aluminium nitrate nonahydrate ($Al(NO_3)_3 \cdot 9\,H_2O$ with 98% purity from Alfa Aesar), citric acid ($C_6H_8O_7$, 99.5+% purity from Alfa Aesar) and poly(ethylene glycol) (PEG-200 from Alfa Aesar) were used as starting compounds. Stoichiometric amount of neodymium oxide was dissolved in distilled water and ultrapure nitric acid (96%). The created neodymium nitrate was recrystallized three times using small volume of distilled water. Then, appropriate quantities of $Cr(NO_3)_3 \cdot 9\,H_2O$ and $Al(NO_3)_3 \cdot 9\,H_2O$ were diluted in distilled water and added to aqueous solution of neodymium nitrate. The mixture was stirred with citric acid and heated up to 90 °C for 1 h in order to create metal complexes. The citric acid, acting as chelating agent was used in double excess in respect to the total amounts of metal ions. Afterwards, PEG-200 was dropped in the solution of metal complexes and stirred for 1 h at 90 °C. PEG-200 and citric acid were used in ratio of 1:1. This step was related with the polyesterification process between organic compounds. After 1 h the reaction mixture was transferred to the crucible and heated up to 250 °C to create the resin. Finally, the nanocrystals were obtained by annealing the resin in air for 8 h at 1000 °C. The powder was homogenised with a rotation speed of 200 rpm for 2 h in isopropanol and the morphologies of the starting powders are shown in Fig. 1a,b.

The ZrB_2 matrix composites with Cr^{3+}/Nd^{3+} doped Al_2O_3 particles were fabricated by spark plasma sintering (SPS) using HPD5 type, FC equipment. Each powder was placed in a graphite die, 20 mm in diameter. The samples were sintered in argon, under 50 MPa. The heating and cooling rate was 200 °C/min and soaking time was 10 min. The sintering temperature was 1550–1600 °C. SPS curves are presented in Fig. 2. A graphite

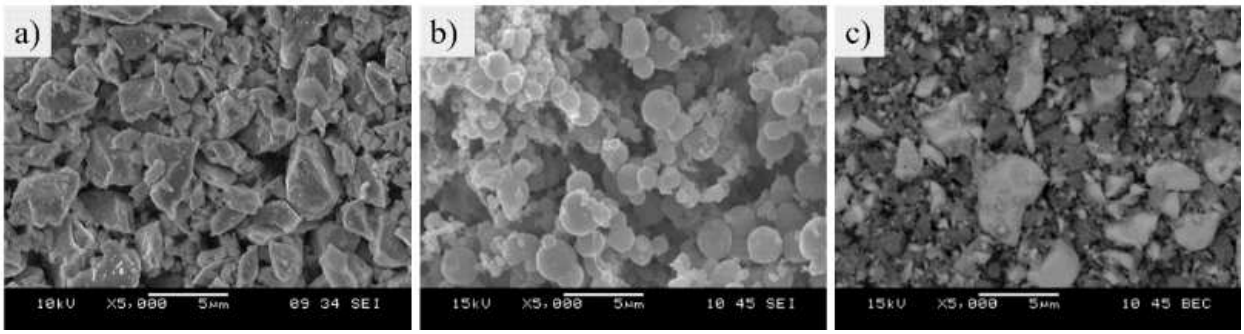

Figure 1. SEM images of the starting: a) ZrB_2, b) Al_2O_3 doped with 1% Cr^{3+} and 1% Nd^{3+} and c) composite ZrB_2/Al_2O_3 ball milled powders

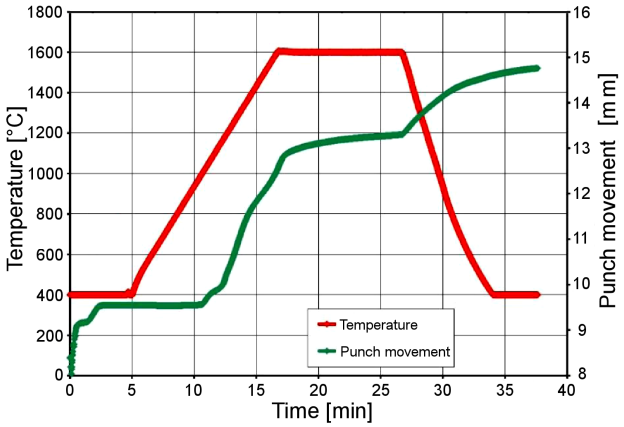

Figure 2. Temperature and punch movement of SPS curves recorded during densification of ZrB_2 matrix composites with 32 wt.% of Cr^{3+}/Nd^{3+} doped Al_2O_3 at 1600 °C, 50 MPa and 10 min

sheet with 0.5 mm in thickness was inserted between the raw material powder and the graphite die to prevent punch scuffing and to facilitate the sintered sample extraction from the matrix. The graphite die was also wrapped with carbon blankets in order to minimize the heat loss during the sintering process.

The produced sintered bodies were tested for physical and mechanical properties. Bulk density was measured using Archimedes' method. XRD patterns were obtained using the PANalytical Empyrean diffractometer with the copper radiation (λ_{Cu} = 1.5406 Å). The quantitative phase analysis of the studied material was carried out using Rietveld refinement and High Score PANalytical software. Microstructure of the materials was studied with a scanning electron microscope (JEOL JSM-6460LV). Young's modulus of the composites was determined by ultrasonic wave transition method measuring the velocity of ultrasonic sound waves passing through the material using an ultrasonic flaw detector (Panametrics Epoch III). The velocities of transversal and longitudinal waves were determined as a ratio of the sample thickness and the relevant transition time. The typical thickness of the studied sample was 3 mm. The hardness and the fracture toughness were determined by the Vickers indentation method using a Future Tech FLC-50VX hardness tester. Applied load was 1 kg for the hardness and 5 and 10 kg in case of fracture toughness. For each sample five indentations were made. The stress intensity factor K_{Ic} was calculated from the length of cracks which developed during a Vickers indentation test using Niihara's equation [16].

The emission spectra were measured using the 445 nm excitation line from a laser diode (LD) and a Silver-Nova Super Range TEC Spectrometer form Stellarnet (1 nm spectral resolution) as a detector. The temperature of the sample, measured in the −190–600 °C temperature range, was controlled using a heating stage from Linkam (0.1 °C temperature stability and 0.1 °C set point resolution).

III. Results and discussion

The characteristic microstructures of the investigated composites are illustrated in Fig. 3. The microstructure is homogeneous for all composites without large technological defects. Only small pores with submicrometre size have been found, whose volume fraction decreased with the increasing content of the Al_2O_3 doped with 1% Cr^{3+} and 1% Nd^{3+} additive. The composites contained ZrB_2 grains with sizes from 0.5 to 3.5 μm and Al_2O_3 grains with sizes from 0.25 to 2.5 μm. Both ZrB_2 and Al_2O_3:(1% Cr^{3+}, 1% Nd^{3+}) grain sizes slightly increased with the increasing weight fraction of the additive (Table 1).

Apparent densities of the pure ZrB_2 and Al_2O_3 are 6.08 and 3.95 g/cm^3, respectively. Thus, the density of the composites decreases with the increased addition of the Cr^{3+}/Nd^{3+} doped Al_2O_3 (Fig. 4).

Table 1. Comparison of the maximum grain size (*MGS*) of sintered ZrB_2 based luminescent composites with addition of 8, 16 and 32 wt.% of aluminium oxide (Al_2O_3 doped with Cr^{3+} and Nd^{3+} ions) and monolithic ZrB_2

Materials	Constituents	*MGS*
monolithic ZrB_2	ZrB_2	3.9 μm
ZrB_2/Al_2O_3 (8 wt.%)	ZrB_2	1.2 μm
	Al_2O_3	0.7 μm
ZrB_2/Al_2O_3 (16 wt.%)	ZrB_2	2.1 μm
	Al_2O_3	1.6 μm
ZrB_2/Al_2O_3 (32 wt.%)	ZrB_2	3.4 μm
	Al_2O_3	2.3 μm

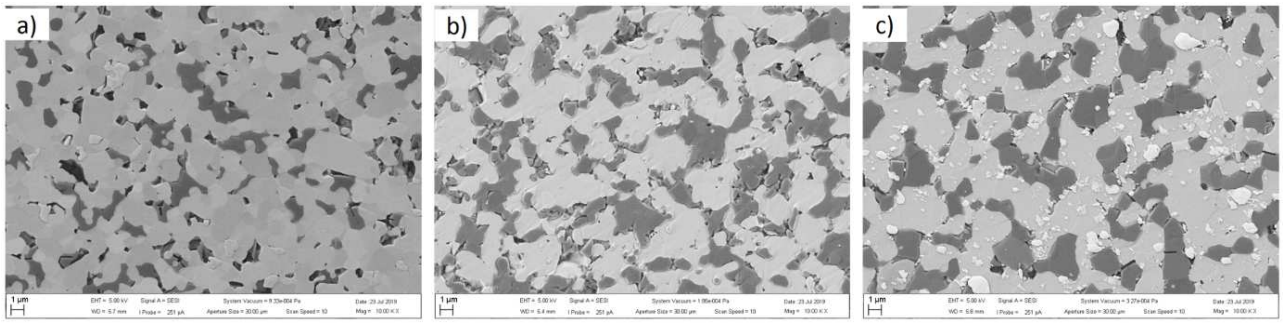

Figure 3. SEM microstructures of ZrB_2 matrix composites with: a) 8, b) 16 and c) 32 wt.% of Cr^{3+}/Nd^{3+} doped Al_2O_3 sintered at 1600 °C

According to the results of the mechanical properties, Vickers hardness *HV*1 and indentation fracture toughness K_{Ic} of the composites improved with an increased addition of the synthesized Cr^{3+}/Nd^{3+} doped Al_2O_3. In Figs. 4a,b and Table 2 the comparison of physical and mechanical properties of the sintered ZrB_2 based luminescent composites with addition of 8, 16 and 32 wt.% of aluminium oxide (Al_2O_3 doped with 1% Cr^{3+} and 1% Nd^{3+} ions) and monolithic ZrB_2 are illustrated. Based on these studies it is obvious that the addition of the Al_2O_3 nanoparticles doped with 1% Cr^{3+} and 1% Nd^{3+} improved the sinterability and the mechanical properties of the composites, compared to the monolithic zirconium diboride. The highest Young's modulus, hardness and fracture toughness were obtained for the ZrB_2 matrix composite with 32 wt.% of Cr^{3+}/Nd^{3+} doped Al_2O_3 with the values of 418 GPa, 16.5 GPa and 5.89 MPa·$m^{1/2}$, respectively.

It is interesting to note (Fig. 4b) that with increasing additive content both the hardness and fracture toughness increase. The increased hardness is possible to explain with the decreasing porosity with the increasing additive content. The increased fracture toughness with increased additive content is probably connected with the slightly increased grain size of the composite (Table 1).

This increased grain size changed the mode of the crack propagation, and significant crack deflection was found in the systems with the highest Al_2O_3 content, which resulted in the improved fracture toughness. Generally, if we have a higher CTE in the dispersed phase, the matrix is under compression and the grains of the secondary phase are under tension, so in our composites tensile stresses should appear in Al_2O_3 and compressive in ZrB_2. Of course, this is just an approximation and simplification. Both of these materials have some

Table 2. Comparison of physical and mechanical properties (calculated density ρ_{cal}, theoretical density ρ_{th}, relative density ρ_r, Young's modulus *E*, Vickers hardness *HV*1, fracture toughness K_{Ic} and sensitivity *S*) of sintered ZrB_2 based luminescent composites with addition of 0, 8, 16 and 32 wt.% of aluminium oxide (Al_2O_3 doped with Cr^{3+} and Nd^{3+} ions)

Material	*T* [°C]	*τ* [min]	ρ_{cal} [g/cm^3]	ρ_{th} [g/cm^3]	ρ_r [g/cm^3]	*E* [GPa]	*HV*1 [GPa]	K_{Ic} [MPa·m$^{1/2}$]	*S* [%]
monolithic ZrB_2	1700	10	5.88 ± 0.01	6.08	96.71	510 ± 34	14.5 ± 0.1	3.91 ± 0.32	-
ZrB_2/Al_2O_3 (8 wt.%)	1600	10	5.60 ± 0.03	5.83	95.99	405 ± 9	14.4 ± 0.5	4.26 ± 0.39	0.90
ZrB_2/Al_2O_3 (16 wt.%)	1600	10	5.28 ± 0.03	5.61	94.17	400 ± 12	15.6 ± 0.5	4.36 ± 0.34	0.95
ZrB_2/Al_2O_3 (32 wt.%)	1600	10	5.20 ± 0.03	5.2	5.2	418 ± 9	16.2 ± 0.3	5.89 ± 0.41	0.98

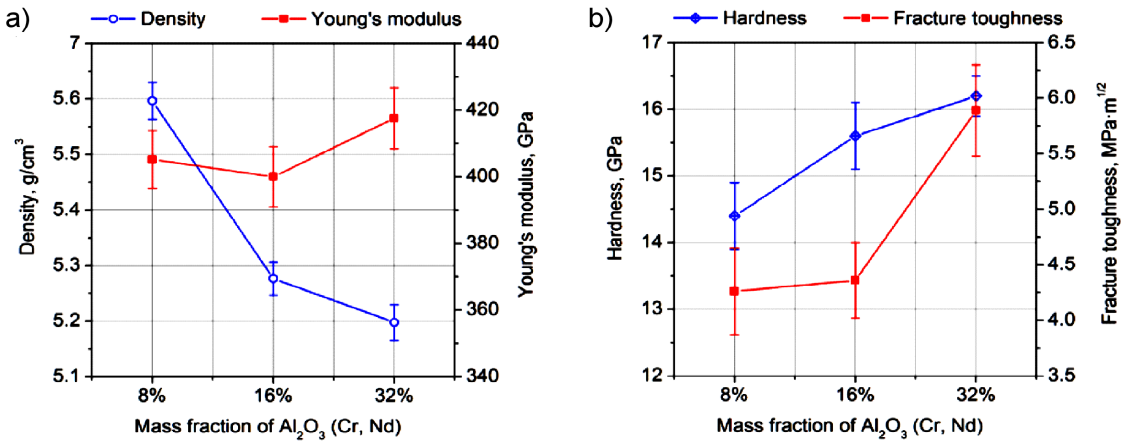

Figure 4. Density and Young's modulus of sintered composites obtained by SPS (a) and Vickers hardness and fracture toughness (b) of sintered composites obtained at 1600 °C

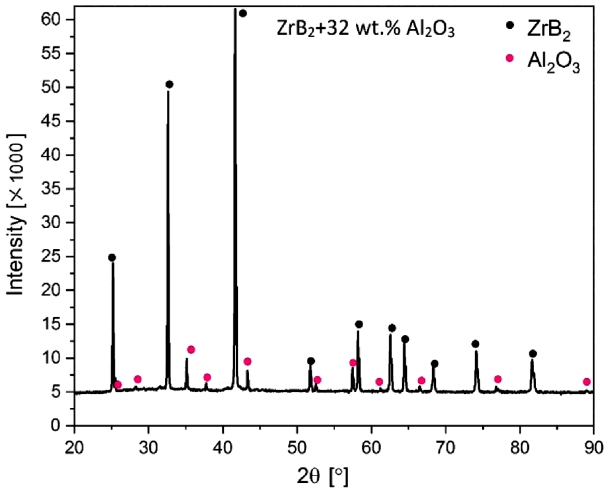

Figure 5. XRD pattern of ZrB_2 matrix composite with 32 wt.% of Cr^{3+}/Nd^{3+} doped Al_2O_3 sintered by SPS at 1600 °C, 50 MPa and 10 min

anisotropy of thermal expansion and the difference in thermal expansion is not significant. The XRD pattern of the obtained ZrB_2 + 32 wt.% Al_2O_3:Nd^{3+} ceramics confirms the lack of the contamination by additional crystallographic phases (Fig. 5). Microscopic observation of the specimens revealed no presence of microcracks.

The luminescent properties of the obtained composites were studied upon 445 nm excitation in a wide range of temperature (−150–500 °C) (Fig. 6a). This wavelength of irradiation provides the emission of Cr^{3+} ions coming from the *d-d* electronic transition from excited states ^2E_g and $^4T_2$ to the ground state $^4A_2$. The $^2E_g \rightarrow {}^4A_2$ and $^4T_2 \rightarrow {}^4A_2$ electronic transitions lead to the generation of two emission bands, namely the narrow emission line with the maximum at 695 nm and the broad emission band, centred at 709 nm, respectively [17]. As it is well known, transition metal ions are strongly susceptible to luminescence thermal quenching. The fact that the excited state parabola is shifted in respect to the ground state one, leads to the appearance of the intersection point. The energy at which this intersection occurs, called activation energy, describes how efficient luminescence of transition metal ion will be quenched at elevated temperatures. In the case of Cr^{3+} ions, which are one of the most extensively investigated, the ^2E excited state parabola intersects with the $^4T_2$ one [11,12,17–20]. Therefore at higher temperatures the non-radiative depopulation leads to the quenching of Cr^{3+} emission intensity. In the case of Al_2O_3 host material the strong crystal field strength is expected. Therefore narrow $^2E \rightarrow {}^4A_2$ emission band at 696 nm is dominant in the spectrum [17]. It can be noticed that the increase of the temperature causes the reduction of luminescent intensity of both emissions, pointing to the phenomenon of luminescence thermal quenching. Due to the intersection between ground and excited states parabola, the provided thermal energy associated with the increase of temperature enabled the activation of non-radiative depopulation of excited states causing the gradual reduction of the emission intensity. However, even at high temperature (400 °C) the intensity of $^2E_g \rightarrow {}^4A_2$ and $^4T_2 \rightarrow {}^4A_2$ electronic transitions are still observed. On the other hand, the intensity of narrow emission line attributed to the $^2E_g \rightarrow {}^4A_2$ transition is definitely more strongly affected by thermal changes than the $^4T_2 \rightarrow {}^4A_2$ one, what is related to the lower activation energy for this energy state. Based on these results, the luminescent intensity ratio (*LIR*), which can be used as a temperature dependent parameter for luminescent thermometry, was defined as follows:

$$LIR = \frac{^2E_g \rightarrow {}^4A_2}{^4T_2 \rightarrow {}^4A_2} = \frac{I(695\,\text{nm})}{I(709\,\text{nm})} \tag{1}$$

The obtained parameter is presented as a function of temperature (Fig. 6b). It can be observed that when the temperature rises the *LIR* decreases in a rapid manner. To quantify the ZrB_2/Al_2O_3 performance for temperature sensing the relative sensitivity parameter (S) was calculated as follows:

$$S = \frac{1}{LIR} = \frac{\Delta LIR}{\Delta T} \times 100\% \tag{2}$$

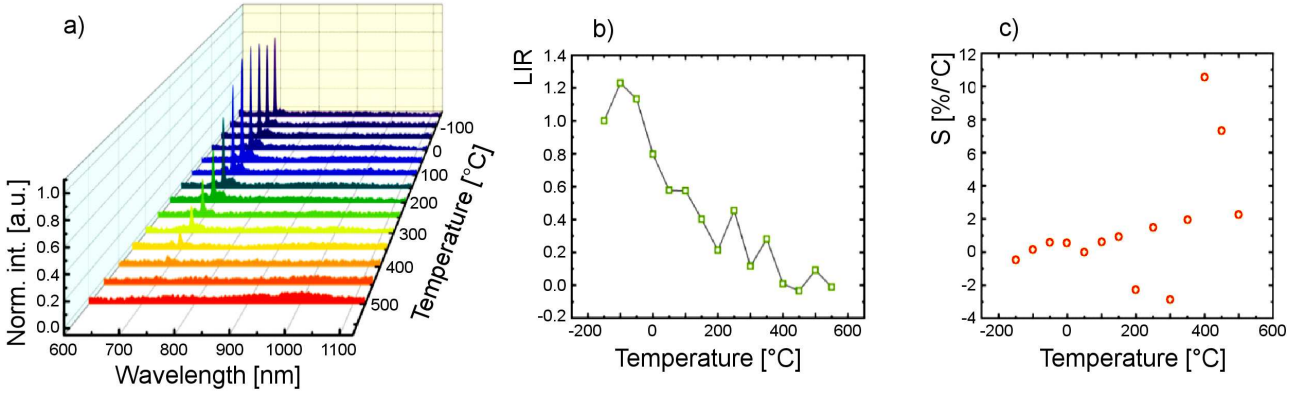

Figure 6. Thermal evolution of emission spectra of ZrB_2 matrix composite with 32 wt.% of Cr^{3+}/Nd^{3+} doped Al_2O_3 (a), Cr^{3+} to Nd^{3+} luminescent intensity ratio as a function of temperature (b) and corresponding S (c)

where ΔLIR represents the change of LIR for ΔT change of temperature.

The relative sensitivity as a function of temperature is presented in Fig. 6c. The negative value of S comes from the definition of ΔLIR. The significant S value of the ZrB_2/Al_2O_3-based luminescent thermometer indicated the capabilities for non-contact temperature controlling and monitoring, simultaneously showing wide operating range. The high values of the S at temperatures above 400 °C result from the low signal intensity. Nevertheless, the obtained S is comparable with the previously described results for other Cr^{3+} based luminescent thermometers [18–20].

In future our research will focus on the development of luminescent advanced ceramics with higher luminescent intensity ratios (*LIR*) which is more stable at higher temperatures. This will contribute to the development of advanced ceramics with wider application ranges, longer life-time and higher reliability.

IV. Conclusions

The aim of the present contribution was to investigate the influence of addition of Al_2O_3 particles doped with 1% Cr^{3+} and 1% Nd^{3+} on the microstructure development, physical, mechanical and luminescent properties of ZrB_2/Al_2O_3 composite. The main results are the following: (i) the addition of the Cr^{3+}/Nd^{3+} doped Al_2O_3 nanoparticles significantly improved the sinterability of the ZrB_2/Al_2O_3 ceramic composites; (ii) the addition of alumina nanoparticles had a positive effect on the mechanical properties of the composite. The hardness increased from 14.5 to 16.2 GPa and the fracture toughness from 3.91 to 5.89 MPa·m$^{1/2}$ in comparison to the values of the monolithic ZrB_2 system; (iii) the composite with the highest additive content showed evident luminescent character with the highest luminescent intensity ratio of approximately 1.2; (iv) the luminescent properties of the Cr^{3+} ions in the ZrB_2/Al_2O_3 composites were used for the first time to implement thermal self-diagnostic feature in ZrB_2-based composites.

Acknowledgements: The authors A.N.D., A. D., J. L. Ł., M. P acknowledge the support of the project FNP – No. POWROTY/2016. The POWROTY/2016-1/3 project is carried out within the Powroty/Reintegration programme of the Foundation for Polish Science co-financed by the European Union under the European Regional Development Fund. Ł.M., K.K. acknowledge "High sensitive thermal imaging for biomedical and microelectronic application" project is carried out within the First Team program of the Foundation for Polish Science co-financed by the European Union under the European Regional Development Fund.

References

1. W.G. Fahrenholtz, G.E. Hilmas, I.G. Talmy, J.A. Zaykoski, "Refractory diborides of zirconium and hafnium", *J. Am. Ceram. Soc.*, **90** (2007) 1347–1364.
2. D. Ghosh, G. Subhash, *Recent Progress in Zr(Hf)B_2 Based Ultrahigh Temperature Ceramics*, Handb. Adv. Ceram. Mater. Appl. Process. Prop. Second Ed., 2013.
3. L. Silvestroni, D. Sciti, C. Melandri, S. Guicciardi, "Tyranno SA3 fiber-ZrB_2 composites. Part II: Mechanical properties", *Mater. Des.*, **65** (2015) 1264–1273.
4. M. Mallik, A.J. Kailath, K.K. Ray, R. Mitra, "Electrical and thermophysical properties of ZrB_2 and HfB_2 based composites", *J. Eur. Ceram. Soc.*, **32** (2012) 2545–2555.
5. P. Barbante, T. Magin, "Fundamentals of hypersonic flight-properties of high temperature gases", RTO AVT Lecture Series on *"Critical Technologies for Hypersonic Vehicle Development"*, van Karman Institut, Rhode-Saint-Genese, Belgium, 2004.
6. W.L. Richards, *Finite-element Analysis of a Mach-8 Flight Test Article Using Nonlinear Contact Elements*, Int. Conf. Contact Mech. Proc., 1997.
7. E. Wuchina, E. Opila, M. Opeka, W. Fahrenholtz, I. Talmy, *UHTCs: Ultra-High Temperature Ceramic Materials for Extreme Environment Applications*, Electrochem. Soc. Interface, 2007.
8. W.G. Fahrenholtz, E.J. Wuchina, W.E. Lee, Y. Zhou, *Ultra-High Temperature Ceramics: Materials for Extreme Environment Applications*, John Wiley & Sons, Inc, New Jersey, USA, 2014.
9. E.W. Neuman, G.E. Hilmas, W.G. Fahrenholtz, "Mechanical behavior of zirconium diboride-silicon carbide-boron carbide ceramics up to 2200 °C", *J. Eur. Ceram. Soc.*, **35** (2015) 463–476.
10. D. Jaque, F. Vetrone, "Luminescence nanothermometry", *Nanoscale*, **4** (2012) 4301.
11. K. Elzbieciak, A. Bednarkiewicz, L. Marciniak, "Temperature sensitivity modulation through crystal field engineering in Ga^{3+} co-doped $Gd_3Al_{5-x}Ga_xO_{12}$:Cr^{3+},Nd^{3+} nanothermometers", *Sensor. Actuat. B Chem.*, **269** (2018) 96–102.
12. Q. Liu, Q.H. Yang, G.G. Zhao, S.Z. Lu, H.J. Zhang, "The thermoluminescence and optically stimulated luminescence properties of Cr-doped alpha alumina transparent ceramics", *J. Alloys Compd.*, **579** (2013) 259–262.
13. K. Bodišová, R. Klement, D. Galusek, V. Pouchlý, D. Drdlík, K. Maca, "Luminescent rare-earth-doped transparent alumina ceramics", *J. Eur. Ceram. Soc.*, **36** (2016) 2975–2980.
14. K. Drdlíková, R. Klement, D. Drdlík, T. Spusta, D. Galusek, K. Maca, "Luminescent Er^{3+} doped transparent alumina ceramics", *J. Eur. Ceram. Soc.*, **37** (2017) 2695–2703.
15. X. Man, L. Yu, S. Li, J. Zhong, "Microstructure and luminescent properties of MgO-Ga_2O_4-SiO_2 glass-ceramics doped with Eu/Ce induced by atmosphere and heated temperature", *J. Non-Cryst. Solids*, **470** (2017) 86–92.
16. K. Niihara, R. Morena, D.P.H. Hasselman, "Evaluation of K_{Ic} of brittle solids by the indentation method with low crack-to-indent ratios", *J. Mater. Sci. Lett.*, **1** (1982) 13–16.
17. P.K. Tawalare, V.B. Bhatkar, S.K. Omanwar, S.V. Moharil, "Cr^{3+} sensitized near infrared emission in Al_2O_3:Cr,Nd/Yb phosphors", *J. Alloys Compd.*, **790** (2019) 1192–1200.
18. K. Elzbieciak, L. Marciniak, "The impact of Cr^{3+} doping on temperature sensitivity modulation in Cr^{3+} doped

and Cr^{3+}, Nd^{3+} co-doped $Y_3Al_5O_{12}$, $Y_3Al_2Ga_3O_{12}$ and $Y_3Ga_5O_{12}$ nanothermometers", *Front. Chem.*, **6** (2018) 424.

19. K. Elzbieciak-Piecka, C. Matuszewska, L. Marciniak, "Step by step designing of sensitive luminescent nanothermometers based on Cr^{3+},Nd^{3+} co-doped $La_{3-x}Lu_xAl_{5-y}Ga_yO_{12}$ nanocrystals", *New J. Chem.*, **43** (2019) 12614–12622.
20. M. Back, E. Trave, J. Ueda, S. Tanabe, "Ratiometric optical thermometer based on dual near-infrared emission in Cr^{3+}-doped bismuth-based gallate host", *Chem. Mater.*, **28** [22] (2016) 8347–8356.